THE ANATOLIAN JOURNAL OF CARDIOLOGY

Official journal of the TURKISH SOCIETY OF CARDIOLOGY

Structural Changes of the Right Fibrous Trigone as a Risk Factor for Conduction Disturbance After Transcatheter Aortic Valve Implantation

ORIGINAL INVESTIGATION

ABSTRACT

Background: The right fibrous trigone, which the His bundle penetrates, is part of the subaortic area adjacent to the membranous septum. Structural alterations of the right fibrous trigone may cause conduction disturbance as a result of compression in this area after transcatheter aortic valve implantation. This study analyzed the hypothesis of whether imaging parameters of the RFT could predict the risk of conduction disturbance after transcatheter aortic valve implantation.

Methods: We retrospectively examined 209 patients who underwent transfemoral transcatheter aortic valve implantationat a tertiary cardiac center. The different valve models were divided into 2 groups: self-expanding valve and balloon-expandable valve. Using pre-procedure computed tomography, we evaluated for the alterations of the right fibrous trigone.

Results: New conduction disturbance was seen in 75 of 209 (35.8%) patients. Receiver operating characteristics plots displayed a right fibrous trigone density of −6 Hounsfield unit for SEV and −16 Hounsfield unit for balloon-expandable valve as the optimal cut-off points for prediction conduction disturbance. In multiple regression analyses, the high density of RFT emerged as an independent predictor of conduction disturbance in both the self-expanding valve (odds ratio: 1.01, 95% CI: 1.01 to 1.02, $P = 0.035$) and balloon-expandable valve (odds ratio: 1.01, 95% CI: 1.01 to 1.03, $P = 0.017$) groups. A shorter membranous septum length and a greater implantation depth were also found to be significantly associated with a higher incidence of conduction disturbance in both transcatheter aortic valve implantation groups.

Conclusion: High density of right fibrous trigone is independently associated with conduction disturbance after transcatheter aortic valve implantation, and its pre-procedure computed tomography evaluation can help predict the new-onset of conduction disturbance.

Keywords: Atrioventricular block, conduction disturbance, left bundle branch block, right fibrous trigone, transcatheter aortic valve implantation

Serkan Aslan[1]
Aysel Türkvatan[2]
Çağdaş Topel[2]
Ahmet Güner[1]
Ali Rıza Demir[1]
Serkan Kahraman[1]
Ömer Çelik[1]
Mehmet Ertürk[1]

[1]*Department of Cardiology, University of Health Sciences, İstanbul Mehmet Akif Ersoy Thoracic and Cardiovascular Surgery Training and Research Hospital, İstanbul, Turkey*
[2]*Department of Radiology, University of Health Sciences, İstanbul Mehmet Akif Ersoy Thoracic and Cardiovascular Surgery Training and Research Hospital, İstanbul, Turkey*

Corresponding author:
Serkan Aslan
✉ serkanaslan84@hotmail.com

Received: September 6, 2021
Accepted: February 7, 2022
Available Online Date: May 11, 2022

Cite this article as: Aslan S, Türkvatan A, Topel Ç, et al. Structural changes of the right fibrous trigone as a risk factor for conduction disturbance after transcatheter aortic valve implantation. *Anatol J Cardiol.* 2022;26(7):532-542.

DOI:10.5152/AnatolJCardiol.2022.987

INTRODUCTION

Conduction disturbances (CDs) such as atrioventricular (AV) block and left bundle branch block (LBBB) are frequent complications after transcatheter aortic valve implantation (TAVI),[1-4] mainly because of the close anatomical relationship between the aortic valvular complex and the AV conduction system.[5,6]

The right fibrous trigone (RFT) is formed by the triangular junction between the aortic valve and the medial parts of the tricuspid and mitral valves, which itself is in fibrous continuity with the adjacent membranous septum (MS) and constitutes the central fibrous body, the strongest part of the cardiac skeleton (Figure 1).[7,8] The AV bundle of His penetrates this area of fibrous tissue and branches into right and left bundle branches as it courses down through the MS, and therefore the bundle of His is in fact in close proximity to the subaortic region and the fibrous part of the left ventricular outflow tract (LVOT).[9,10] It is this relationship that allows us to understand why the radial force applied by the prosthesis stent frame of the transcatheter heart valve to the annulus and LVOT can

Copyright@Author(s) - Available online at anatoljcardiol.com.
Content of this journal is licensed under a Creative Commons Attribution-NonCommercial 4.0 International License.

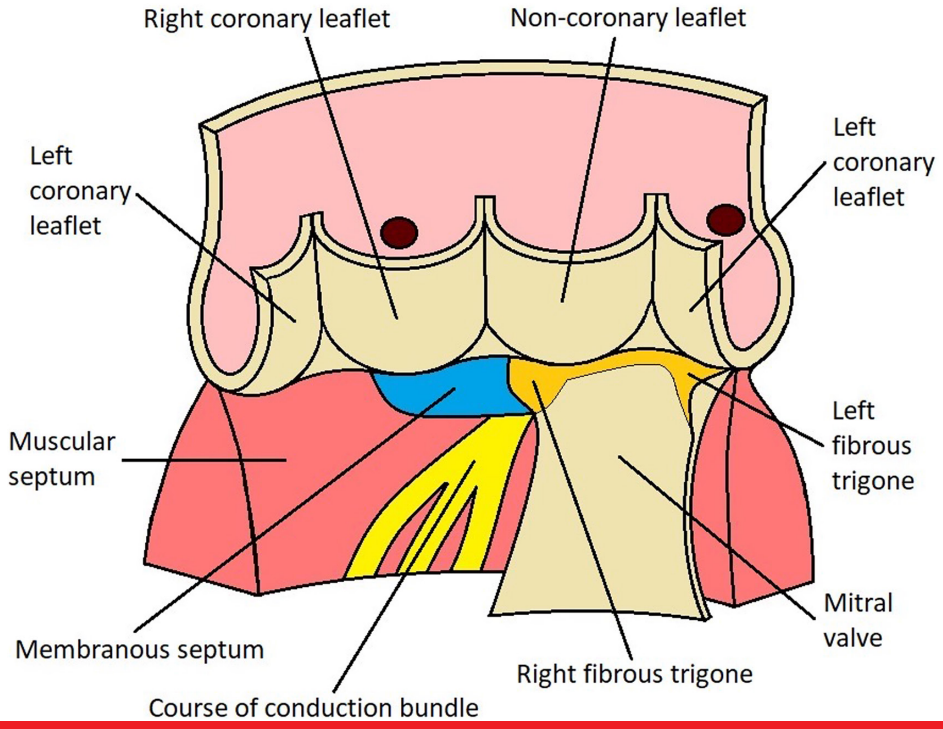

Figure 1. Anatomic relationship between the aortic valve and the cardiac conduction system. The drawing of the aortic root opened through the left ventricular outflow tract region illustrates the fibrous continuities between the right fibrous trigone (orange) and the membranous septum (blue). The atrioventricular conduction axis is shown in yellow and penetrates through this fibrous area.

lead to high-degree AV block or intraventricular conduction abnormalities. We, therefore, hypothesized that the structural changes in RFT are an anatomic predictor of the risk of high-degree AV block and new-onset LBBB associated with TAVI. There is no relevant data available to support this hypothesis in the previous studies.

The purpose of this study is to investigate whether structural characteristics of the RFT evaluated with pre-TAVI computed tomography (CT) would predict high-grade AV block and LBBB, independent of procedural- or device-related factors.

HIGHLIGHTS

- Right fibrous trigone density assessed by computed tomography is significantly associated with an increased risk of conduction disturbance after transcatheter aortic valve implantation, regardless of valve type.
- Right fibrous trigone density of ≥ −6 Hounsfield unit for self-expanding valve and ≥ −16 Hounsfield unit for balloon-expandable valve were as the optimal cutoff points for prediction conduction disturbance.
- The high density of right fibrous trigone emerged as an independent predictor for the occurrence of new conduction disturbance in both the self-expanding valve and balloon-expandable valve.
- Shorter membranous septum length and deeper implantation depth emerged as other significant predictors.

METHODS

Study Population and Design

We retrospectively analyzed the CT angiography datasets of 263 consecutive patients with severe symptomatic aortic stenosis undergoing TAVI in our institution between January 2016 and February 2021. Patients with preexisting or postoperative transient LBBB (n=28), prior permanent pacemaker (PPM) (n=8), periprocedural death (n=13), implantation of 2 prostheses (n=3), and low-quality image of CT scans (n=2) were excluded from the study. The final data analysis of the study included a total of 209 patients.

This report focused exclusively on the relationship between CD and parameters of RFT, and the identification of predictors of the CD. The primary outcome of this study was the occurrence of CD following the procedure. Conduction disturbance was defined as a composite of new-onset persistent LBBB or high-degree AV block. The different valve models were divided into 2 groups: self-expanding valve (SEV) and balloon-expandable valve (BEV). Each TAVI group was divided into 2 groups, patients with new-onset CD and those without CD. Initial demographic and clinical information, anatomical, ECG, and post-procedure characteristics were evaluated for each TAVI valve design.

Outcomes were reported using the Valve Academic Research Consortium (VARC)-3 criteria.[11] The study was conducted in accordance with the principles of the Helsinki Declaration and approved by the Local Institutional Review Board (Date: February 23, 2021; Decision No: 2021/16).

TAVI Procedure

All patients were evaluated in detail by the heart team, including a cardiologist and by a cardiac surgery, and found the high risk for valve surgery. All TAVI procedures were performed in a hybrid catheterization laboratory and conscious sedation was commonly used in TAVI procedures. The following transcatheter valve designs were used: CoreValve Evolut R (Medtronic, Minneapolis, Minn, USA), Portico (St. Jude Medical, St. Paul, Minneapolis, Minn, USA), Sapien XT (Edwards Lifesciences, Irvine, Calif, USA), and Myval (Meril Life Sciences Private Ltd., Gujarat, India). Prostheses were sized using manufacturer's recommendations. Post-dilatation under rapid pacing was considered in the case of remaining moderate or severe paravalvular aortic regurgitation and/or prosthesis under expansion. A temporary pacemaker was placed as a backup for high-grade AV block, when necessary. Implantation depth was measured using fluoroscopic images in the projection chosen for deployment and defined as the distance from the deepest portion of the noncoronary cusp to the intraventricular end of the bioprosthesis, as previously described.[12]

Electrocardiogram Assessment

Standard 12-lead electrocardiograms (ECGs) were recorded from all patients at baseline (within 24 hours before the procedure), immediately after the procedure, and at discharge. Each ECG tracing analysis included rhythm, heart rate, QRS morphology, PR interval, and duration of the QRS complex.[13] The following CD was recorded: postoperative high-degree AV block (defined as third degree AV block or Mobitz Type II second degree AV block), new-onset LBBB. The criteria to diagnose a complete LBBB on the ECG were defined as a QRS duration of >120 ms, dominant S wave in V1, broad monophasic R wave in lateral leads (I, aVL, V5-V6), and an R peak time >60 ms in V5 or V6.[13] New-onset persistent LBBB was defined as LBBB that first appeared after TAVI and was persisted at the time of discharge or >7 days after the index procedure in case of prolonged hospitalization according to the VARC-3.[11]

CT ASSESSMENT

CT Images Acquisition

All patients were examined using a 320-row CT scanner (Aquilion ONE, Toshiba Medical Systems, Otawara, Japan) with a gantry rotation time of 350 ms. The TAVI protocol consists of a prospectively ECG-gated (with 20-70% of the R-R interval) axial 1-beat acquisition of the aortic root and heart followed by a non-ECG-gated CT angiography of the thorax, abdomen, and pelvis using a single contrast bolus. The imaging data were obtained during intravenous injection of 50-80 mL of the contrast agent (Iohexol, Omnipaque 350 mg/mL; GE Healthcare Milwaukee, Wis, USA) at an injection rate of 4-5 mL/s and followed by a 30-50 mL saline chaser with the same injection rate. The scanning delay was determined with a bolus tracking technique by placing the region of interest (ROI) in the descending aorta and setting the trigger threshold to 180 Hounsfield unit (HU). The tube voltage and tube current depend on the body mass index (BMI) of the patients. Tube voltage was 100 kV (BMI ≤30 kg/m^2) or 120 kV (BMI >30 kg/m^2) and tube current was 320-480 mA. The CT acquisitions were reconstructed to 0.5 mm in thickness with an iterative reconstruction algorithm.

CT Images Analysis

The aortic root images were independently reviewed by two experienced radiologists, unaware of the clinical data for the presence of CD using a dedicated workstation (Vitrea version 6.4, Vital Images, USA) to allow for multiplanar reformations. To measurement of the aortic root dimensions, a double oblique transverse view (en face view of the aortic valve) was created in the systolic phase (20-40%) of the cardiac cycle since aortic root dimensions are commonly larger in systole. The annulus was reviewed throughout the available phases of the cardiac cycle and the phase giving the largest annulus dimensions with adequate image quality was visually determined. To create a double oblique transverse view, the cross-hairs were centered in the aortic valve in the axial, coronal, and sagittal views and aligned along the long axis of the aortic root in the coronal and sagittal views. The aortic annulus was defined as the virtual basal ring containing the most caudal attachments of the 3 aortic valve cusps on a double-oblique transverse view. The perimeter of the virtual basal ring was traced manually. Planimetry yielded maximum/minimum diameters, luminal area, and perimeter. The mean annular diameter was calculated by a workstation software based on these measurements. The aortic annulus eccentricity was calculated as follows: 1-(minimum diameter/maximum diameter). Calcification of the basal ventricular septum was determined by CT using a semi-quantitative model (0=no calcification, 1=presence of calcification), as previously described.[14] The length of the MS was measured as the distance between the aortic annular plane and the crest of the muscular interventricular septum in the coronal view as previously described.[14]

To identify the RFT, the short-axis images of the LVOT were reconstructed using a 3-chamber view image (Figure 2). The RFT was identified as a triangle-shaped fibrofatty tissue between the medial parts of the tricuspid and mitral valves and the nadir of the hinge-line of the non-coronary aortic cusp. The RFT measurements were made in the mid-diastolic phase of the cardiac cycle (70%) since the image quality of the RFT is better in the diastolic phase. The measurement of the area and the density of the RFT were performed at the maximal diameter of the triangular fibrofatty tissue between the medial parts of the AV valves and the hinge point of the noncoronary cusp. To measure the area of the RFT, the boundaries of this triangular fibrofatty tissue were manually traced. The planimetry method was used to calculate the area of the RFT. To measure the density (CT attenuation) of the RFT, a free-hand ROI was drawn in this triangular fibrofatty tissue (Figure 3). While drawing the ROI, the edges of the RFT were avoided to prevent partial volume averaging. The ROI measurements were repeated 3 times for each case, and the median density was obtained.

Statistical Analysis

Since there is no similar study in the literature, a pilot study was carried out to calculate the sample size. Patients who underwent TAVI were scanned retrospectively and 20

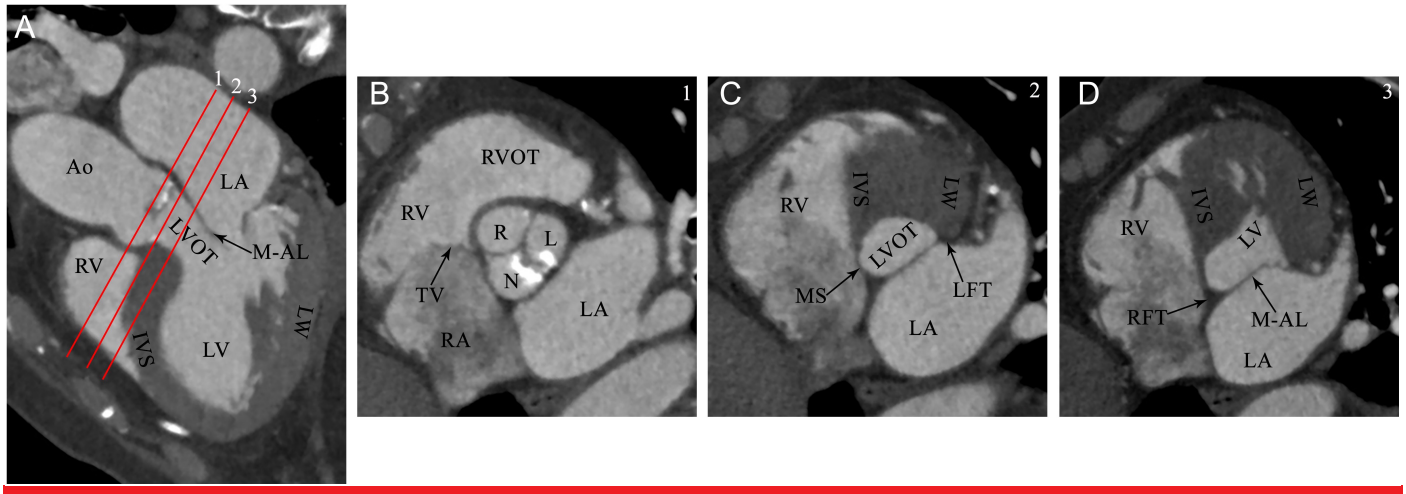

Figure 2. (A) Three-chamber view and (B-D) short-axis images of the left ventricular outflow tract (LVOT) show the fibrous component of the LVOT. Short axis images of the LVOT, displayed from superior to inferior, were reconstructed using the 3-chamber view image. The right fibrous trigone (RFT) is seen as a triangle-shaped fibrofatty tissue between the medial parts of the tricuspid and mitral valves and the nadir of the hinge line of the non-coronary cusp (N) of the aortic valve. Ao, aorta; IVS, interventricular septum; L, left coronary cusp; LA, left atrium; LFT, left fibrous trigone; LV, left ventricle; LW, lateral wall; M-AL, mitral anterior leaflet; MS, membranous septum; R, right coronary cusp; RA, right atrium; RV, right ventricle; RVOT, right ventricular outflow tract; TV, tricuspid valve.

patients with post-TAVI CD and 20 patients without CD were identified. While the mean RFT density was −27.5 ± 44.2 HU in the group with no conduction defects in the measurements performed, it was found to be 2.1 ± 43.7 HU in the group observed. According to the power analysis made by taking these values into account, the sample number was determined to be 158 with 95% power and 1% margin of error. The statistical analyses were performed using the SPSS software, version 24.0 (SPSS Inc., Chicago, Ill, USA). Preprocedure parameters, procedural data, and post-procedure outcomes were compared between patients with or without CD. The normal distribution hypothesis was tested by graphical (histograms and probability curves) and numerical methods (Kolmogorov–Simirnov's and Shapiro–Wilk). Continuous variables are reported as the mean ± standard deviation (SD) or median [interquartile range (IQR)] and were compared using the Student's *t*-test or Mann–Whitney U-test was used as appropriate. Categorical variables are presented as frequencies and percentages and differences between proportions were calculated by using the chi-square or Fisher exact test as appropriate. The independent predictors of new-onset persistent CD were determined using a binary logistic regression model including variables with *P*-value ≤ .10 in the univariable analysis. The 95% CI was used to estimate the precision of the odds ratio (OR) in each model. The receiver operating characteristics (ROC) curve was used to determine the thresholds of continuous variables predicting the presence of CD. All tests were 2-tailed with $P < .05$ considered significant.

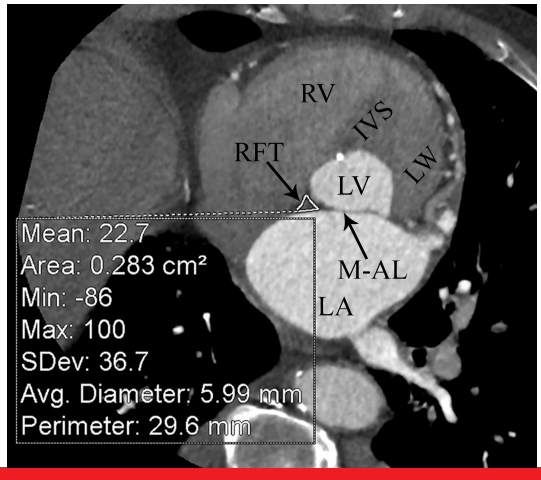

Figure 3. An 83-year-old male patient with high-degree AV block. In the short-axis image of the left ventricular outflow tract, the density of the right fibrous trigone (RFT) was measured with a free-hand ROI as a mean of 22.7 HU. IVS, interventricular septum; LA, left atrium; LV, left ventricle; LW, lateral wall; M-AL, mitral anterior leaflet; RV, right ventricle.

RESULTS

Patients' Characteristics for SEV and BEV

The baseline characteristic in the SEV and BEV groups according to whether or not CD develops are reported in Table 1. In the BEV group (mean age: 77.6 ± 7.1 years; male: 39.1%), clinical comorbidities were well balanced in the study population. The most common comorbidities in patients with aortic stenosis (AS) were hypertension (65.5%) and coronary artery disease (55.4%). These results were consistent with those in the SEV group; however, in that group, peripheral artery disease and cerebrovascular disease were numerically higher compared with the BEV group. Baseline patient demographic, clinical, and preoperative echocardiographic characteristics were comparable in both the SEV and BEV groups.

Table 1. Baseline Characteristics of the Study Population According to Conduction Disturbance

	Self-Expanding Valve				Balloon-Expandable Valve			
		Conduction Disturbance				Conduction Disturbance		
Parameters	**Total (n = 117)**	**No (n = 69)**	**Yes (n = 48)**	***P***	**Total (n = 92)**	**No (n = 63)**	**Yes (n = 29)**	***P***
Demographic and clinical characteristics								
Age (years)	80.1 ± 6.4	79.6 ± 6.2	80.9 ± 6.7	.283	77.6 ± 7.1	77.4 ± 8.1	78.2 ± 4.6	.626
Sex (male)	43 (36.8)	21 (30.9)	22 (44.9)	.121	36 (39.1)	28 (44.4)	8 (27.6)	.124
Coronary artery disease	84 (71.8)	49 (71.0)	35 (72.9)	.822	51 (55.4)	35 (55.6)	16 (55.2)	.973
COPD	29 (24.8)	18 (26.1)	11 (22.9)	.696	32 (34.8)	22 (34.9)	10 (34.5)	.967
Diabetes	44 (37.6)	26 (37.7)	18 (37.5)	.984	36 (39.1)	24 (38.1)	12 (41.4)	.764
Chronic kidney disease	33 (28.2)	17 (24.6)	16 (33.3)	.304	24 (26.1)	15 (23.8)	9 (31.0)	.463
Hypertension	77 (65.8)	42 (60.9)	35 (72.9)	.177	52 (65.5)	37 (58.7)	15 (51.7)	.529
Previous CABG	31 (26.5)	18 (26.1)	13 (27.1)	.904	16 (17.4)	12 (19.0)	4 (13.8)	.537
Peripheral vascular disease	28 (23.9)	14 (20.3)	14 (29.2)	.268	15 (16.3)	10 (15.9)	5 (17.2)	1.0
Cerebrovascular disease	7 (6.0)	4 (5.8)	3 (6.2)	1.0	2 (2.2)	1 (1.6)	1 (3.4)	.533
STS score	6.0 (4.0-8.7)	6.0 (4.0-9.0)	5.8 (4.0-7.9)	.433	6.0 (4.0-9.0)	5.4 (4.0-9.0)	6.1 (4.5-9.0)	.980
Echocardiographic characteristics								
LVEF (%)	54.6 ± 9.8	55.6 ± 8.9	53.0 ± 10.8	.159	55.7 ± 9.6	55.9 ± 10.4	55.3 ± 7.6	.785
Aortic valve area (cm^2)	0.71 ± 0.13	0.72 ± 0.14	0.70 ± 0.12	.322	0.74 ± 0.13	0.74 ± 0.13	0.74 ± 0.14	.949
Maximum aortic transvalvular velocity (m/s)	4.3 ± 0.4	4.43 ± 0.47	4.33 ± 0.50	.255	4.41 ± 0.57	4.36 ± 0.62	4.52 ± 0.41	.231
Maximum aortic transvalvular gradient (mm Hg)	77.5 ± 17.3	78.4 ± 16.1	76.1 ± 19.2	.489	78.5 ± 20.1	76.9 ± 21.6	82.0 ± 16.3	.262
Mean aortic transvalvular gradient (mm Hg)	48.3 ± 11.8	48.7 ± 11.5	47.7 ± 12.4	.646	50.2 ± 12.3	49.5 ± 13.3	51.7 ± 9.5	.425
sPAP (mm Hg)	40.1 ± 10.9	39.9 ± 12.2	40.4 ± 9.4	.832	39.7 ± 14.2	39.4 ± 14.8	40.6 ± 13.0	.746
Electrocardiographic characteristics								
Ventricular rate (beats per minute)	74.4 ± 13.0	75.2 ± 11.9	73.2 ± 14.5	.406	75.9 ± 13.2	75.5 ± 13.2	76.9 ± 13.3	.646
Sinus rhythm	93 (79.5)	58 (84.1)	35 (72.9)	.142	77 (83.7)	50 (79.4)	27 (93.1)	.132
Atrial fibrillation	24 (20.5)	11 (15.9)	13 (27.1)	.142	15 (16.3)	13 (20.6)	2 (6.9)	.132
PR interval (ms)	167.5 ± 31.4	166.9 ± 31.1	168.6 ± 32.6	.806	169.7 ± 32.6	170.1 ± 30.6	168.8 ± 36.5	.868
QRS duration (ms)	95.6 ± 16.7	94.1 ± 16.4	97.9 ± 17.0	.224	93.5 ± 17.8	93.7 ± 19.5	93.1 ± 13.5	.867
First-degree AV block	15 (16.1)	10 (16.4)	5 (15.6)	.924	12 (13.0)	8 (12.7)	4 (13.8)	1.0
Complete right bundle branch block	12 (10.3)	4 (5.8)	8 (16.7)	.057	8 (8.7)	4 (6.3)	4 (13.8)	.255

Values represent mean ± SD, n (%) or median (interquartile range).
AV, atrioventricular block; CABG, coronary artery bypass grafting; COPD, Chronic obstructive pulmonary disease; LVEF, left ventricular ejection fraction; sPAP, systolic pulmonary artery pressure; STS, Society of Thoracic Surgeons.

Data from the 12-lead ECG before TAVI are displayed in Table 1. In the preoperative ECG data 170 out of the 209 patients (81.3%) showed sinus rhythm, whereas 39 of the patients (18.7%) displayed atrial fibrillation. The presence of prior atrial fibrillation was 20.5% in the SEV group and was numerically higher in patients with CD, but it was not statistically significant (27.1% vs. 15.9%, *P* = .142). In the entire cohort (n = 209), the prevalence of CD as determined by VARC-3 definition after TAVI was as follows: new-onset LBBB (25.4%) and high-grade AV block (10.5%). Overall, 78 patients (37.3%) developed new-onset LBBB after TAVI, and 25 patients recovered from new-onset LBBB (transient) before discharge or within 7 days after TAVI. The high-grade AV block rate was significantly higher in patients with RBBB (25% in its favor when compared to no RBBB 9%, *P* = .027).

Procedural Data, CT, and Fluoroscopic Angiographic Measurements

According to CT parameters, RFT density was significantly higher in patients with CD in both TAVI groups than in patients without CD (for BEV, 13.4 ± 31.1 vs. −20.5 ± 52.4 HU, *P* = .002; for SEV, 5.4 ± 37.5 vs. −16.7 ± 44.2 HU, *P* = .005), whereas RFT area did not differ statistically between both BEV and SEV groups (*P* = .140; *P* = .489, respectively). When both study populations were stratified into quartiles based on RFT density, patients within the two highest quartiles had

a more frequent incidence of CD when compared with the two lowest quartiles group (for BEV, $P = .005$; for SEV, $P = .011$) (Figure 4). In the overall BEV group, compared with patients with no CD, those with CD had shorter MS length (6.6 ± 1.4 vs. 7.8 ± 1.3 mm, $P < .001$) and greater implantation depth (8.3 ± 1.6 vs. 6.1 ± 1.9 mm, $P < .001$). Calcification in the basal septum was more likely to develop CD following TAVI (41.4% vs. 17.5%, $P = .014$). In the SEV group, patients with CD had significantly shorter MS length (7.2 ± 1.3 vs. 7.9 ± 1.3 mm, $P = .011$), greater implantation depth (8.9 ± 2.6 vs. 7.1 ± 2.0 mm, $P < .001$), and more presence of calcification in LVOT (45.8% vs. 24.6%, $P = .017$) compared with those without CD. No differences in conscious sedation, contrast use, and balloon post-dilatation were observed between patients with CD and those without CD in either the BEV or SEV group (Table 2). In both populations, there were no differences in aortic annular or LVOT measurements. Inter- and intra-observer variability of CT data was less than 5%.

Predictors of Conduction Disturbances

The results of the univariable and multivariable analyses of predictors of subsequent CD for the entire population of the study are displayed in Table 3. On univariable analysis, several parameters were significantly related to subsequent CD: shorter MS length, greater implantation depth, high density of RFT, the presence of calcification in the basal septum, longer QRS duration, and prior atrial fibrillation. The multivariable analysis revealed high density of RFT (OR: 1.01, 95% CI: 1.01 to 1.02, $P = .003$) as an independent predictor for new-onset CD. The other independent predictors for CD were of shorter MS length (OR: 0.56, 95% CI: 0.42 to 0.74, $P < .001$) and greater implantation depth (OR: 1.44, 95% CI: 1.22 to 1.70, $P < .001$). We also observed a borderline significant trend toward a higher CD rate in patients with basal septal calcifications ($P = .058$).

On univariable analysis, the predictors of CD were also given separately for the balloon-expandable and self-expanding valves (Table 4). In the multivariable model, the high density of RFT was found to be significantly associated with a higher incidence of CD in both SEV and BEV groups (SEV, OR: 1.01, 95% CI: 1.01 to 1.02, $P = .035$; BEV, OR: 1.01, 95% CI: 1.01 to 1.03, $P = .017$) (Table 5). As shown in Figure 5, ROC plots display an RFT density of −6 HU for SEV and −16 HU for BEV as the optimal cutoff points for prediction CDs, with negative predictive values of 74.6% and 93.9%, respectively.

DISCUSSION

Three major findings of the current study are (1) high-density of RFT as assessed by CT was identified as an independent anatomic predictor of CD after TAVI regardless of the different valve designs; (2) RFT density ≥ −15 HU for BEV and ≥ 6 HR for SEV were optimal cutoff value for predicting CD; (3) shorter MS length and deeper implantation depth emerged as independent predictors of CD.

The emergence of conduction disorders such as newly developed LBBB or high-grade AV block after TAVI is mainly explained by the close anatomical relationship between the

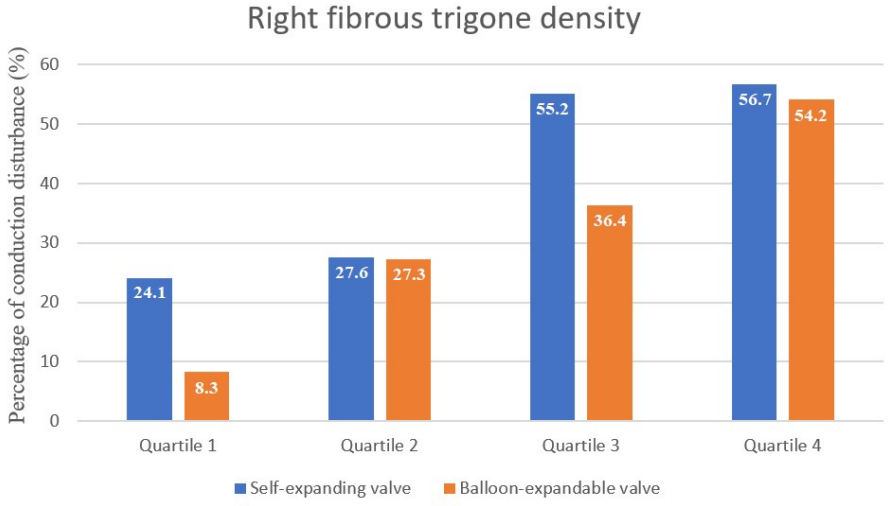

Quartile range	< 25	25 - 50	51 – 75	76 - 100
RFT density (HU) for SEV	≤ -36	-35 to -6	-5 to 23	≥ 24
RFT density (HU) for BEV	≤ -38	-37 to 0	1 to 3	≥ 33

Abbreviations: BEV, balloon-expandable valve; HU, Hounsfield unit; RFT, right fibrous trigone; SEV, self-expanding valve.

Figure 4. Incidence of conduction disturbances according to quartiles of RFT density.

Table 2. CT and Procedural Characteristics of Patients According to Conduction Disturbance

	Self-Expanding Valve				Balloon-Expandable Valve			
		Conduction Disturbance				Conduction Disturbance		
Parameters	**Total (n = 117)**	**No (n = 69)**	**Yes (n = 48)**	***P***	**Total (n = 92)**	**No (n = 63)**	**Yes (n = 29)**	***P***
CT Characteristics								
Annulus perimeter (mm)	75.3 ± 6.0	74.8 ± 6.1	75.9 ± 6.0	.369	79.1 ±7.0	79.2 ± 7.5	78.8 ± 5.9	.795
Annulus, perimeter-derived diameter (mm)	23.9 ± 1.9	23.8 ± 1.9	24.1 ± 1.9	.380	25.1 ± 2.2	25.1 ± 2.4	25.1 ± 1.9	.919
Annulus area (mm^2)	437.6 ± 71.4	433.6 ± 72.9	443.3 ± 69.6	.475	487.2 ± 90	489.3 ± 97.3	482.5 ± 74.9	.739
Annulus, area-derived diameter (mm)	23.5 ± 1.9	23.4 ± 1.9	23.7 ± 1.9	.412	24.7 ± 2.2	24.8 ± 2.4	24.5 ± 1.8	.506
Minimum annulus size (mm)	20.7 ± 1.9	20.6 ± 1.9	20.7 ± 1.8	.807	21.7 ± 2.4	21.7 ± 2.6	21.6 ± 2.0	.875
Maximum annulus size (mm)	26.8 ± 2.1	26.7 ± 2.1	27.1 ± 2.2	.341	26.9 ± 2.4	27.0 ± 2.4	26.6 ± 2.4	.521
Mean annulus size (mm)	23.7 ± 1.8	23.6 ± 1.8	23.9 ± 1.9	.517	24.3 ± 2.2	24.4 ± 2.3	24.1 ± 2.0	.620
Minimum LVOT size (mm)	19.4 ± 2.3	19.4 ± 2.1	19.4 ± 2.5	.946	20.1 ± 2.7	20.2 ± 2.9	19.7 ± 2.2	.423
Maximum LVOT size (mm)	27.3 ± 2.4	27.4 ± 2.3	27.1 ± 2.6	0.643	27.2 ± 2.3	27.3 ± 2.3	27.0 ± 2.5	.636
Mean LVOT size (mm)	23.4 ± 2.2	23.4 ± 2.0	23.3 ± 2.3	0.787	23.6 ± 2.3	23.7 ± 2.5	23.4 ± 2.0	.611
Mean diameter of the sinus valsalva (mm)	30.8 ± 2.7	31.3 ± 2.6	30.1 ± 2.8	0.843	31.4 ± 2.9	31.8 ± 3.0	30.2 ± 2.8	.778
Ascending aorta (mm)	34.2 ± 3.2	34.1 ± 3.5	34.3 ± 2.9	.765	36.1 ± 4.7	35.5 ± 4.2	37.5 ± 5.7	0.094
Membranous septum length (mm)	7.6 ± 1.3	7.9 ± 1.3	7.2 ± 1.3	.011	7.4 ± 1.4	7.8 ± 1.3	6.6 ± 1.4	<.001
Implantation depth (mm)	7.8 ± 2.4	7.1 ± 2.0	8.9 ± 2.6	<.001	6.8 ± 2.1	6.1 ± 1.9	8.3 ± 1.6	<.001
Right fibrous trigone area (mm^2)	97.4 ± 35.6	99.4 ± 33.7	94.7 ± 38.4	.489	106.4 ± 47.4	101.4 ± 41.5	117.2 ± 57.4	.140
Right fibrous trigone density (HU)	−7.6 ± 42.8	−16,7 ± 44.2	5.4 ± 37.5	.005	-9.8 ± 49.2	−20.5 ± 52.4	13.4 ± 31.1	.002
Eccentricity index	0.23 ± 0.05	0.23 ± 0.05	0.23 ± 0.05	.747	0.19 ± 0.06	0.20 ± 0.07	0.18 ± 0.06	.427
Calcification in basal septum	39 (33.3)	17 (24.6)	22 (45.8)	.017	23 (25.0)	11 (17.5)	12 (41.4)	.014
Procedural characteristics								
Conscious sedation	108 (92.3)	64 (92.8)	44 (91.7)	.828	51 (55.4)	35 (55.6)	16 (55.2)	.973
Opaque (ml)	150 (120-200)	140 (120-190)	150 (120-228)	0.167	120 (95-150)	130 (100-150)	110 (90-145)	.079
Valve type								
Sapien XT				.694	84 (91.3)	59 (70.2)	25 (29.8)	.255
Myval					8 (8.7)	4 (50.0)	4 (50.0)	
Portico	93 (79.5)	54 (58.1)	39 (41.9)					
Evolut-R	24 (20.5)	15 (62.5)	9 (37.5)					
Balloon post-dilatation	59 (50.4)	38 (55.1)	21 (43.8)	.228	33 (35.9)	22 (34.9)	11 (37.9)	.780

Values represent mean ± SD, n (%) or median (interquartile range).
CT, computed tomography; HU, Hounsfield unit; LVOT, left ventricular outflow tract.

aortic valve and the basic structures of the heart conduction system. Briefly, the RFT, which is in fibrous continuity with the MS, is located just below the noncoronary sinus, and therefore RFT is very close to the subaortic region of the LVOT.[5–7,15,16] As described by Tawara, the AV node is directly adjacent to the central fibrous body of the heart. The AV node continues as the bundle of His. The AV conduction axis penetrates the RFT before the bundle branches off. It then penetrates the

Table 3. Predictors of New-Onset Persistent Conduction Disturbance on Binary Logistics Regression Analysis

Variables	Univariable Analysis			Multivariable Analysis		
	OR	95% CI	*P*	OR	95% CI	*P*
Age	1.02	0.98-1.07	.177			
Male	0.80	0.45-1.42	.456			
Coronary artery disease	1.12	0.62-2.02	.705			
Diabetes	1.04	0.58-1.86	.877			
Chronic kidney disease	1.50	0.80-2.79	.199			
Hypertension	1.24	0.69-2.22	.466			
Prior CABG	1.03	0.53-2.02	.914			
Prior atrial fibrillation	1.08	0.53-2.23	.816			
Membranous septum length	0.57	0.45-0.73	<.001	0.56	0.42-0.74	<.001
Implantation depth	1.54	1.32-1.80	<.001	1.44	1.22-1.70	<.001
Right fibrous trigone area	1.00	0.99-1.01	.635			
Right fibrous trigone density	1.01	1.00-1.02	<.001	1.01	1.00-1.02	.003
Eccentricity	1.14	0.14-93.73	.951			
Calcification in basal septum	2.93	1.59-5.42	.001	2.03	0.97-4.22	.058
Balloon post-dilatation	1.49	0.85-2.64	.162			
Pre-operative QRS duration	1.02	1.00-1.04	.009	1.01	0.98-1.03	.469
First-degree AV block	1.02	0.43-2.42	.966			
Complete right bundle branch block	2.86	1.11-7.35	.029	2.19	0.46-10.25	.319

CABG, coronary artery bypass grafting; OR, odds ratio.

Table 4. Binary Logistics Regression Analysis to Determine the New-Onset Conduction Disturbance for Balloon-Expandable and Self-Expanding Valves

Variables	Self-Expanding Valve			Balloon-Expandable Valve		
	OR	95% CI	*P*	OR	95% CI	*P*
Age	1.01	0.95-1.07	.604	1.01	0.95-1.08	.622
Male	1.82	0.85-3.91	.123	0.56	0.22-1.42	.226
Coronary artery disease	1.37	0.60-3.15	.449	1.01	0.41-2.46	.973
Diabetes	0.69	0.32-1.49	.349	1.14	0.46-2.81	.764
Chronic kidney disease	1.45	0.64-3.27	.365	1.44	0.54-3.82	.465
Hypertension	1.82	0.82-4.05	.140	0.75	0.31-1.82	.529
Prior CABG	1.01	0.43-2.30	.994	0.88	0.28-2.79	.836
Prior atrial fibrillation	2.32	0.93-5.78	.071	0.28	0.06-1.35	.115
Membranous septum length	0.65	0.48-0.89	.007	0.47	0.31-0.71	<.001
Implantation depth	1.41	1.17-1.69	<.001	1.80	1.37-2.36	<.001
Right fibrous trigone area	0.99	0.98-1.01	.329	1.01	0.99-1.01	.142
Right fibrous trigone density	1.01	1.01-1.02	.011	1.01	1.01-1.02	.003
Eccentricity	3.06	0.01-2.52	.744	0.06	<0.001-48.6	.423
Calcification in basal septum	2.37	1.07-5.24	.032	3.33	1.24-8.93	.016
Valve type						
Portico[a]	1.91	0.72-5.05	.190			
Myval[b]				1.18	0.88-1.59	.250
Balloon post-dilatation	0.63	0.30 -1.33	.229	1.22	0.49-3.05	.667
Pre-operative QRS duration	1.02	0.99-1.04	.097	1.02	0.99-1.05	.107
First-degree AV block	0.94	0.29-3.04	.924	1.10	0.30-3.99	.885
Complete right bundle branch block	3.25	0.91-11.49	.067	2.36	0.54-10.19	.250

[a]Compared to Evolut-R.
[b]Compared to Sapien XT.
CABG, coronary artery bypass grafting; OR, odds ratio.

Table 5. Binary Logistics Regression Analysis to Determine the New-Onset Conduction Disturbance for Balloon-Expandable and Self-Expanding Valves

Variables	Self-Expanding Valve			Balloon-Expandable Valve		
	OR	95% CI	*P*	OR	95% CI	*P*
Membranous septum length	0.55	0.38-0.80	.002	0.55	0.35-0.86	.009
Implantation depth	1.35	1.10-1.65	.004	1.54	1.17-2.03	.002
Right fibrous trigone density	1.01	1.01-1.02	.035	1.01	1.01-1.03	.017
Calcification in basal septum	1.62	0.64-4.05	.303	3.24	0.91-11.52	.069
QRS duration	1.02	0.99-1.04	.101			
Prior atrial fibrillation	2.07	0.71-6.01	.180			

HU, Hounsfield unit; OR, odds ratio.

MS and ascends to the LVOT located at the top of the muscular ventricular septum.[17] This anatomical relationship has generated interest in understanding the anatomy of the aortic valve complex, particularly concerning the conduction system. In the present study, we hypothesized that the structural changes of the RFT involved in the formation of the fibrous support of the aortic root may affect the structural integrity of the aortic root after TAVI and consequently increase the interaction of TAVI prostheses with the conduction system, damage the conduction system, and result in a higher new PPM implantation rate. Moreover, the current data indicated that RFT density varies among patients with aortic stenosis referred to as TAVI, and this anatomical variation is indeed clearly associated with the risk of new-onset LBBB and high-grade AV block. As a result of its anatomical location, high-density RFT is a potent and independent pretreatment predictor of CD. RFT density of ≥−6 HU for SEV and ≥−16 HU for BEV were the optimal threshold for predicting CD and separated high-risk patients from the rest of the cohort, supporting the hypothesis that the insertion of the TAVI in patients with high-density RFT could seriously damage the conduction system.

To the best of our knowledge, there are no data available for the role of RFT density in predicting TAVI-related high-grade AV block and LBBB in patients with aortic stenosis. Assessment of the RFT density based on pre-operative CT can help predict mechanical stress on the AV conduction axis and the risk of CD. We also believe that our data may help to further elucidate the TAVR-related CD and provide more information on clinical decision-making and risk stratification for patients undergoing TAVI.

We consider that there are several possible explanations for RFT density differences between patients. First, the RFT is mainly composed of adipose (fat) and supportive connective tissue components. Inter-individual variation in the amount and structure of each component may determine how susceptible these structures are to injury during TAVI. Large amounts of dense connective tissue may play an important role in communicating the radial force applied by the TAVI valve to the conduction paths and may expose patients to a higher risk of TAVI-induced CD. Second, perhaps more importantly, we think that the accumulation of calcium-containing crystals in the RFT increases the mechanical damage caused by direct compression of the conduction system in this area by the TAVI prosthesis. Our hypothesis that calcium-containing crystal deposition may lead to CDs is supported by data previously obtained by other authors.[18,19] Moreover, in another study by Tohno et al in which age-related changes of elements in both the right and left fibrous trigones of the human heart were examined, they found that calcium gradually increased in both rights and left fibrous trigones with aging.[20] Future research should focus on confirming the findings of our study and exploring the role of calcium-containing crystals and structural variation in RFT.

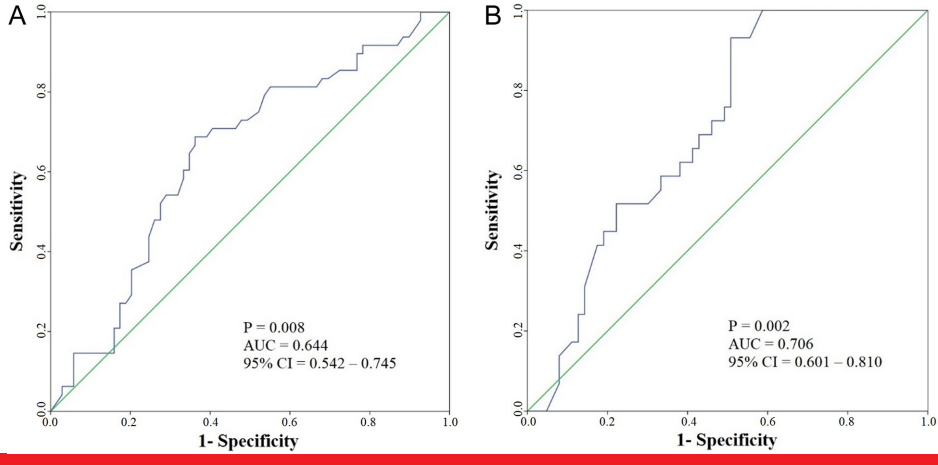

Figure 5. Receiver operating characteristic curves of right fibrous trigone as a predictor of conduction disturbance for both valve designs. AUC, area under the curve.

Mechanisms of CD after TAVI are multifactorial. Several factors can affect the interaction between the valve and the delivery system, including the results of the procedure, such as basic conduction abnormalities, LVOT anatomy, and implant depth.[21,22] Several investigators have assessed the pre-operative and post-operative risk factors predictive of post-TAVI CD and demonstrated the role of implantation depth,[22] MS length,[14] and baseline ECG abnormalities.[4] Computed tomography evaluation of the MS has been shown to provide useful information about CD risk.[14] Moreover, most recent reports of the proposed TAVI prior to CT evaluation recommend analyzing the MS using a standard coronal view.[23,24] In our study, shorter MS length was found to be significantly associated with a higher incidence of CD in both TAVI groups. After TAVI, implantation depth is now considered an important risk factor and an independent predictor of damage to the AV conduction axis.[25] Similar to previously published literature knowledge, in our study, high implantation depth emerged as the strongest independent preprocessing predictor of a higher degree of AV block and LBBB after TAVI regardless of the different valve designs.

Self-expanding valve has been associated with more frequent incidences of CD (18-65%) than BEV (4-30%) at hospital discharge and with LBBB being the most common significant CD following TAVI.[21,26-28] The reasons for the higher rate of CD in self-expanding valves have been attributed to the valve design and the potential of deeper implantation into the LVOT. This may result in more mechanical compression of the RFT and more severe injury to the AV node and left bundle branch. In our study, the rate of 25.4% NP-LBBB and 10.5% high-grade AV block appeared similar to those reported previously. In addition, the incidence of CD was 1.5-fold higher in patients receiving the SEV (41.0%) than in those receiving BEV (31.5%).

Study Limitations

The present study had several limitations. The first and most obvious limitation of the current study is that it was a retrospective and single-center observational study with a relatively small cohort.

Left ventricular outflow tract calcification could not be quantified using the Agatstone score, which reflects the total area of calcium deposits and calcium density, as non-contrast cardiac calcium score examination was not performed prior to CT angiography, which is not an essential component of the TAVI.[29] Calcification of the basal ventricular septum was determined by cardiac CT angiography using a semi-quantitative model as previously described.[14] However, we feel confident of our model being robust and statistically valid, and it identifies important factors for CD following TAVI, that may be relevant to decision-making. Second, the PPM requirement is not included in the CD, as the decision for PPM implantation may differ between physicians and more broadly between institutions. For this reason, we determined the LBBB and high-degree AV block as a more accurate result on the ECG before discharge. Third, ECG interpretation for new-onset LBBB was limited from the TAVI procedure to discharge and was defined as any new LBBB after TAVI that was maintained at the time of discharge. However, the new-onset LBBB may resolve not only during the hospital stay but also over a longer period of time. This report focuses specifically on the occurrence of CD after TAVI and therefore the resolution of LBBB after discharge was not examined.

CONCLUSION

Alterations in structural characteristics of the RFT in TAVI patients are significantly associated with an increased risk of CD. Right fibrous trigone density, as assessed by CT, is an independent powerful pre-procedural predictor of CD occurring after TAVI, regardless of valve type. Therefore, preoperative evaluation of RFT anatomy may help predict the risk of CD after TAVI. Membranous septum length and implantation depth emerged as other significant predictors. For verifying the current findings, future studies should focus on identifying the pathophysiological mechanisms between RFT and CD.

Ethics Committee Approval: Ethical committee approval was received from the Ethics Committee of University of Health Sciences, Istanbul Mehmet Akif Ersoy Thoracic and Cardiovascular Surgery Training and Research Hospital (approval number: 2021-16).

Informed Consent: Written informed consent was obtained from all participants who participated in this study.

Peer-review: Externally peer-reviewed.

Author Contributions: Concept – S.A., M.E.; Design – S.A., A.T., Ö.Ç., M.E.; Supervision – A.T., A.G., Ö.Ç., M.E.; Fundings – None; Materials – S.A., A.T., Ç.T., A.R.D., S.K., Ö.Ç.; Data collection &/or processing – S.A., A.T., Ç.T., A.R.D., S.K.; Analysis &/or interpretation – S.A., A.G., A.R.D., S.K.; Literature search – S.A., Ç.T., A.G., A.R.D.; Writing – S.A., A.T., A.G.; Critical review – A.T., S.K., Ö.Ç., M.E.

Declaration of Interests: The authors declare that they have no competing interests.

Funding: This study received no funding.

REFERENCES

1. van Rosendael PJ, Delgado V, Bax JJ. Pacemaker implantation rate after transcatheter aortic valve implantation with early and new-generation devices: a systematic review. *Eur Heart J*. 2018;39(21):2003-2013. [CrossRef]
2. Regueiro A, Abdul-Jawad Altisent O, Del Trigo M, et al. Impact of new-onset left bundle branch block and periprocedural permanent pacemaker implantation on clinical outcomes in patients undergoing transcatheter aortic valve replacement: A systematic review and meta-analysis. *Circ Cardiovasc Interv*. 2016;9(5):e003635. [CrossRef]
3. Siontis GC, Jüni P, Pilgrim T, et al. Predictors of permanent pacemaker implantation in patients with severe aortic stenosis undergoing TAVR: a meta-analysis. *J Am Coll Cardiol*. 2014;64(2):129-140. [CrossRef]
4. Chen S, Chau KH, Nazif TM. The incidence and impact of cardiac conduction disturbances after transcatheter aortic valve replacement. *Ann Cardiothorac Surg*. 2020;9(6):452-467. [CrossRef]
5. Mangieri A, Montalto C, Pagnesi M, et al. TAVI and post procedural cardiac conduction abnormalities. *Front Cardiovasc Med*. 2018;5:85. [CrossRef]

6. Kawashima T, Sato F. Visualizing anatomical evidences on atrioventricular conduction system for TAVI. *Int J Cardiol*. 2014;174(1):1-6. [CrossRef]
7. Saremi F, Sánchez-Quintana D, Mori S, et al. Fibrous skeleton of the heart: anatomic overview and evaluation of pathologic conditions with CT and MR imaging. *RadioGraphics*. 2017;37(5):1330-1351. [CrossRef]
8. Mori S, Fukuzawa K, Takaya T, et al. Clinical cardiac structural anatomy reconstructed within the cardiac contour using multidetector-row computed tomography: left ventricular outflow tract. *Clin Anat*. 2016;29(3):353-363. [CrossRef]
9. Saremi F, Hassani C, Sánchez-Quintana D. Septal atrioventricular junction region: comprehensive imaging in adults. *RadioGraphics*. 2016;36(7):1966-1986. [CrossRef]
10. Anderson RH, Yanni J, Boyett MR, Chandler NJ, Dobrzynski H. The anatomy of the cardiac conduction system. *Clin Anat*. 2009;22(1):99-113. [CrossRef]
11. VARC-3 WRITING COMMITTEE, Généreux P, Piazza N, et al. Valve Academic Research Consortium 3: updated endpoint definitions for aortic valve clinical research. *Eur Heart J*. 2021;42(19):1825-1857. [CrossRef]
12. Petronio AS, Sinning JM, Van Mieghem N, et al. Optimal implantation depth and adherence to guidelines on permanent pacing to improve the results of transcatheter aortic valve replacement with the Medtronic CoreValve system: the CoreValve prospective, international, post-market ADVANCE-II study. *JACC Cardiovasc Interv*. 2015;8(6):837-846. [CrossRef]
13. Surawicz B, Childers R, Deal BJ, et al. AHA/ACCF/HRS recommendations for the standardization and interpretation of the electrocardiogram: part III: intraventricular conduction disturbances: a scientific statement from the American Heart Association Electrocardiography and Arrhythmias Committee, Council on Clinical Cardiology; the American College of Cardiology Foundation; and the Heart Rhythm Society. Endorsed by the International Society for Computerized Electrocardiology. *J Am Coll Cardiol*. 2009;53(11):976-981. [CrossRef]
14. Hamdan A, Guetta V, Klempfner R, et al. Inverse relationship Between membranous septal length and the risk of atrioventricular block in patients undergoing transcatheter aortic valve implantation. *JACC Cardiovasc Interv*. 2015;8(9):1218-1228. [CrossRef]
15. Wilczek K, Reguła R, Bujak K, Chodór P, Długaszek M, Gąsior M. Conduction disturbances after transcatheter aortic valve implantation procedures - predictors and management. *Postepy Kardiol Interwencyjnej*. 2016;12(3):203-211. [CrossRef]
16. Piazza N, de Jaegere P, Schultz C, Becker AE, Serruys PW, Anderson RH. Anatomy of the aortic valvar complex and its implications for transcatheter implantation of the aortic valve. *Circ Cardiovasc Interv*. 2008;1(1):74-81. [CrossRef]
17. Das Reizleitungssystem de Saugetierherzens TS. *Eine Anatomich- Hisologische Studie Uber Das Atrioventricularbundel und Die Purkinjeschen Faden*. Jena: Verlag von Gustav Fischer; 1906.
18. Takamoto T, Popp RL. Conduction disturbances related to the site and severity of mitral anular calcification: a 2-dimensional echocardiographic and electrocardiographic correlative study. *Am J Cardiol*. 1983;51(10):1644-1649. [CrossRef]
19. Montemurro D, Ronzani G, Defilippi G, Pizzuti A, Brusca A. Conduction disorders and sites of calcification of the mitral ring: 2-dimensional echocardiographic study. *G Ital Cardiol*. 1986;16(4):308-312.
20. Tohno S, Azuma C, Tohno Y, et al. Increases of calcium, phosphorus, and magnesium in both the right and left fibrous trigones of human heart with aging. *Biol Trace Elem Res*. 2007;119(2):111-119. [CrossRef]
21. Zaid S, Sengupta A, Okoli K, et al. Novel anatomic predictors of new persistent left bundle branch block After Evolut transcatheter aortic valve implantation. *Am J Cardiol*. 2020;125(8):1222-1229. [CrossRef]
22. Pollari F, Großmann I, Vogt F, et al. Risk factors for atrioventricular block after transcatheter aortic valve implantation: a single-centre analysis including assessment of aortic calcifications and follow-up. *Europace*. 2019;21(5):787-795. [CrossRef]
23. Maeno Y, Abramowitz Y, Kawamori H, et al. A highly predictive risk model for pacemaker implantation After TAVR. *JACC Cardiovasc Imaging*. 2017;10(A):1139-1147. [CrossRef]
24. Chen YH, Chang HH, Liao TW, et al. Membranous septum length predicts conduction disturbances following transcatheter aortic valve replacement. *J Thorac Cardiovasc Surg*. 2020;S0022-5223(20):32230-32233. [CrossRef]
25. Alperi A, Muntané-Carol G, Freitas-Ferraz AB, et al. Overcoming the transcatheter aortic valve replacement Achilles heel: conduction abnormalities-a systematic review. *Ann Cardiothorac Surg*. 2020;9(6):429-441. [CrossRef]
26. Finkelstein A, Steinvil A, Rozenbaum Z, et al. Efficacy and safety of new-generation transcatheter aortic valves: insights from the Israeli transcatheter aortic valve replacement registry. *Clin Res Cardiol*. 2019;108(4):430-437. [CrossRef]
27. Husser O, Kessler T, Burgdorf C, et al. Conduction abnormalities and pacemaker implantations After SAPIEN 3 Vs Sapien XT prosthesis aortic valve implantation. *Rev Esp Cardiol (Engl Ed)*. 2016;69(2):141-148. [CrossRef]
28. Walther T, Manoharan G, Linke A, et al. Incidence of new-onset left bundle branch block and predictors of new permanent pacemaker following transcatheter aortic valve replacement with the Portico™ valve. *Eur J Cardiothorac Surg*. 2018;54(3):467-474. [CrossRef]
29. Blanke P, Weir-McCall JR, Achenbach S, et al. Computed tomography imaging in the context of transcatheter aortic valve implantation (TAVI)/transcatheter aortic valve replacement (TAVR): an expert consensus document of the Society of Cardiovascular Computed Tomography. *JACC Cardiovasc Imaging*. 2019;12(1):1-24. [CrossRef]